



# CHORUS

This is the accepted manuscript made available via CHORUS. The article has been published as:

## Epsilon-Near-Zero Modes for Tailored Light-Matter Interaction

Salvatore Campione, Sheng Liu, Alexander Benz, John F. Klem, Michael B. Sinclair, and Igal Brener

Phys. Rev. Applied **4**, 044011 — Published 20 October 2015

DOI: [10.1103/PhysRevApplied.4.044011](https://doi.org/10.1103/PhysRevApplied.4.044011)

# Epsilon-near-zero modes for tailored light-matter interaction

Salvatore Campione<sup>1,2,\*,\$</sup>, Sheng Liu<sup>1,2,\$</sup>, Alexander Benz<sup>1,2</sup>, John F. Klem<sup>1</sup>, Michael B. Sinclair<sup>1</sup>, and Igal Brener<sup>1,2,†</sup>

<sup>1</sup>Sandia National Laboratories, Albuquerque NM 87185 USA

<sup>2</sup>Center for Integrated Nanotechnologies (CINT), Sandia National Laboratories, Albuquerque NM 87185 USA

<sup>\$</sup>These authors contributed equally to this work and are joint first authors

**Abstract**—Epsilon-near-zero (ENZ) modes arising from condensed matter excitations such as phonons and plasmons are a new path for tailoring light-matter interactions at the nanoscale. Complex spectral shaping can be achieved by creating such modes in nanoscale semiconductor layers and controlling their interaction with multiple, distinct, dipole resonant systems. Examples of this behavior are presented at mid-infrared frequencies for ENZ modes that are strongly coupled to metamaterial resonators and *simultaneously* strongly coupled to semiconductor phonons or quantum well intersubband transitions, resulting in double and triple polariton branches in transmission spectra. For the double polariton branches case, we find that the best strategy to maximize the Rabi splitting is to use a combination of a doped layer supporting an ENZ feature and a layer supporting ISTs, with overlapping ENZ and IST frequencies. This design flexibility renders this platform attractive for low-voltage tunable filters, light-emitting diodes, and efficient nonlinear composite materials.

PACS NUMBERS: 78.67.Pt; 78.67.De; 78.67.-n; 78.20.-e

## 1. Introduction

The pursuit of natural and artificial epsilon-near-zero (ENZ) response has led to intriguing optical properties [1], including supercoupling [2-4], highly directional beaming [5-8], optical nanocircuits [9], optical switching and bistability [10, 11], and cloaking devices [12]. In this work, we aim to tailor light-matter interactions at the nanoscale by using fundamental condensed matter excitations such as plasmons and phonons that lead to spectral regions of ENZ behavior. Deeply subwavelength films are known to support coupled surface modes — ENZ modes — at the frequency where the film’s dielectric permittivity vanishes [13-15]. We propose here a system whose spectral properties are controlled by the interaction between the ENZ modes of semiconductor nanolayers and multiple, distinct, dipole resonant systems. In particular, we consider ENZ modes that are strongly coupled to metamaterial (MM) resonators and *simultaneously* strongly coupled to semiconductor phonons or quantum well intersubband transitions (ISTs). Such three-way coupling

leads to double and triple polariton branches in transmission and reflection spectra.

Prior work has shown the realization of double polariton branches by coupling MMs to quantum well ISTs [16-23], ENZ modes [24, 25], and optical phonons [26, 27]. More generally, MM structures interacting with semiconductor heterostructures supporting excitations such as phonons, plasmons, and electronic transitions, offer a platform for tunable spectral behavior that is attractive for low-voltage tunable filters [28], innovative efficient nonlinear elements [29-31], and light-emitting diodes [32]. Our objective here is to show the advantages of using ENZ modes for tailoring the spectral response of strongly coupled systems.

The platform discussed in this paper is represented by the block diagram in Fig. 1(a), which describes a system where ENZ modes interact with two, distinct, dipole resonant systems. In this work, one of the resonant systems will always be MM resonators, while the other will be either semiconductor phonons or quantum well ISTs. Note that both the ENZ mode and the ISTs require  $z$ -polarized fields, which are readily generated in the near field of the MM resonators. Of course one can envision a more general system in which the ENZ modes interact with more than two dipole resonances, but the analysis provided here is sufficient to understand the achievable properties. In some cases, the ENZ mode and the second dipole resonance coexist in the same nanolayer, as happens in the case of semiconductor optical phonons shown in Fig. 1(b). This implementation is however limited by the inability to adjust the optical phonon frequency and the detuning between the ENZ mode and the phonon resonance. This limitation can be overcome by using two layers, one supporting the required ENZ modes and the other supporting the second dipole resonance as shown in Fig. 1(c) for the case of quantum well ISTs. This is the most flexible case, in which the relative positions and resonance frequencies of the ENZ and dipole layers determine the complex spectral response of the strongly coupled system.

In what follows, we will analyze three representative cases of three-way coupling using ENZ modes. In Section 2, we examine as “Case 1” the simultaneous strong coupling of ENZ modes to MM resonators and optical phonons where we clearly observe the generation of three polariton branches. This is in contrast to the results of [26] where the polariton

\* sncampi@sandia.gov

† ibrener@sandia.gov

branch due to the ENZ mode was barely visible. In Section 3, we investigate as “Case 2” the strong coupling between the ENZ mode and quantum well ISTs, for the case where the frequencies of the ENZ mode and ISTs are detuned. This case helps us to unravel the physics of strong coupling with optical phonons. Finally, in Section 4 we analyze as “Case 3” the case where the frequencies of the ENZ modes and ISTs are degenerate.

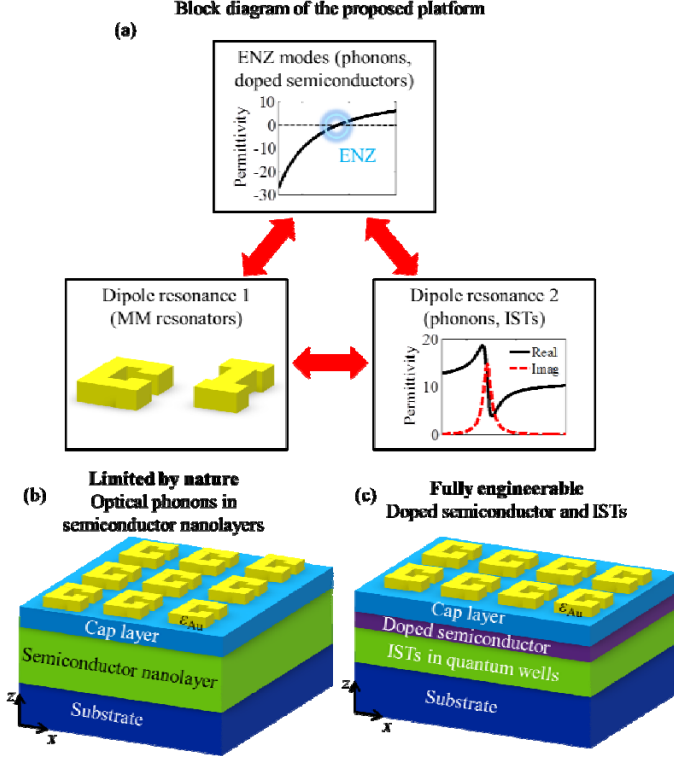


Fig. 1. ENZ modes arising from condensed matter excitations such as phonons and plasmons represent a new path for tailoring light-matter interactions at the nanoscale. (a) Block diagram of the proposed platform comprising ENZ modes and two dipole resonances. The ENZ modes will be simultaneously coupled to MM resonators and a second resonant system which will either be: (b) optical phonons occurring in the ENZ layer; or (c) quantum well ISTs occurring in a separate layer. MM resonators are shown on top of each semiconductor heterostructure in panels (b) and (c).

## 2. Case 1: Simultaneous strong coupling of ENZ modes to MM resonators and optical phonons

We investigate in this section the spectral properties of a system comprising 100-nm-thick gold split-ring resonator MMs and a semiconductor heterostructure as in Fig. 2(a) containing a 3-nm-thick GaAs cap layer, a 10-nm-thick AIAs layer, and a GaAs substrate. The relative permittivity of gold  $\epsilon_{\text{Au}}$  is described using a Drude model [33] with parameters extracted from spectral ellipsometry measurements of a 100 nm-thick gold film which yield a plasma angular frequency of  $2\pi \times 2060 \times 10^{12}$  rad/s and a damping rate of  $2\pi \times 10.9 \times 10^{12}$  rad/s. The AIAs nanolayer supports optical phonons at  $\sim 360$   $\text{cm}^{-1}$  (see Fig. 2(b)), and the ENZ region associated with this resonance occurs at  $\sim 400$   $\text{cm}^{-1}$ . Note that since the ENZ frequency arises as a result of the phonon

resonance, its frequency is fixed for a given material, thus providing limited capabilities with respect to the system analyzed in Secs. 3 and 4. Because of the spectral separation of the phonon and ENZ frequencies, we anticipate that both the phonons and the ENZ modes will strongly couple to the MMs and lead to polariton splitting. Note that the particular geometry used for the MM resonators is not important, so long as the bare cavity resonance is controlled by the size of the resonators.

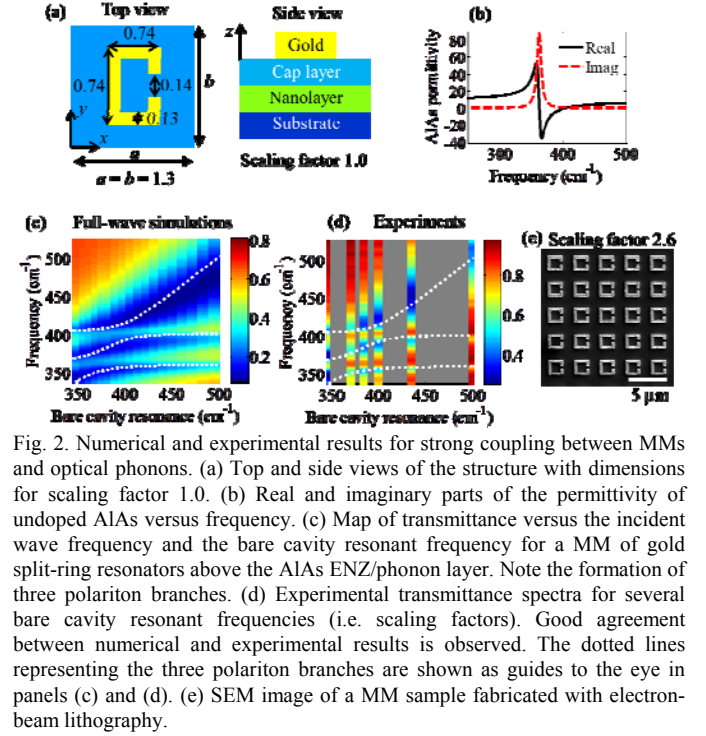


Figure 2(c) shows the transmittance as a function of incident wave frequency and bare cavity resonance frequency, obtained from full-wave simulations [34] of the split-ring resonator array on top of the AIAs nanolayer. To generate the transmittance map in Fig. 2(c), we simulated a set of MMs for which all the spatial dimensions of the MM of split-ring resonators are scaled by a common scaling factor that varied between 2.0 and 2.9 relative to the dimensions shown in Fig. 2(a). For each scaling factor, we performed a full-wave simulation of the MM without the AIAs layer to determine the bare cavity resonance frequency as the location of minimum transmittance. Next, we performed simulations including the AIAs nanolayer and plotted the obtained transmittance spectra versus the bare cavity frequency. A similar procedure was used to generate all the full-wave simulation transmittance maps shown in this manuscript. We observe clearly that the transmittance spectra exhibit three polariton branches, a signature of strong coupling of the MM resonators to both the phonon resonance (around  $360$   $\text{cm}^{-1}$ ) and the ENZ mode (around  $400$   $\text{cm}^{-1}$ ).

Next, we experimentally verify the predictions of Fig. 2(c). Similar to the full-wave simulations, we geometrically scale the MM dimensions which allow us to sweep the bare cavity resonance across the ENZ and phonon resonance frequencies

and map out the three polariton branches. The MM is defined by electron beam lithography directly on top of the semiconductor heterostructure. A Ti/Au (5/100 nm) layer is evaporated followed by a standard lift-off process. A scanning electron micrograph (SEM) image of a fabricated sample is reported in Fig. 2(e). The transmittance spectra were measured at room temperature using a Bruker IFS66v, and are shown in Fig. 2(d). Two transparency windows, i.e. three polariton branches, are clearly visible at 360 and 400  $\text{cm}^{-1}$  in agreement with full-wave simulations.

As mentioned earlier, the implementation presented in Fig. 2 is limited by the inability to adjust the optical phonon frequency and the detuning between the ENZ mode and the phonon resonance. In the next sections, we propose an alternative implementation to overcome this limitation.

### 3. Case 2: Fully engineerable system with detuned ENZ mode and IST frequencies

The results of Sec. 2 demonstrate that optical phonons can be utilized to tailor the behavior of photonic structures and opens up new directions for their usage in strong coupling scenarios. However, optical phonon frequencies are defined by intrinsic material properties and can hardly be modified. To circumvent this problem we separate the functionality and use a doped semiconductor layer to create the ENZ modes, and a multi-quantum well layer containing ISTs as the second dipole resonance. This system is fully tunable since the ENZ frequency can be adjusted by varying the doping level, and the IST frequencies can be tuned by modifying the quantum well design. In particular, we adopt the structure shown in the inset of Fig. 3 which consists of a MM array of dogbone resonators (gold, 100 nm thick) placed on top of a multilayered substrate comprising: an  $\text{Al}_{0.48}\text{In}_{0.52}\text{As}$  cap layer (30 nm thick) with  $\epsilon_c = 10.23$ ; a doped  $\text{In}_{0.53}\text{Ga}_{0.47}\text{As}$  layer exhibiting an ENZ effect; a quantum well slab containing 20 repeat units of an  $\text{In}_{0.53}\text{Ga}_{0.47}\text{As}/\text{Al}_{0.48}\text{In}_{0.52}\text{As}$  heterostructure (12.5/20 nm) supporting ISTs at a frequency of  $\approx 24.2$  THz; and an InP substrate with  $\epsilon_s = 9.3$ . The relative permittivity of the doped InGaAs,  $\epsilon_{\text{ENZ}}$ , is described with a Drude model

$$\epsilon_{\text{ENZ}} = \epsilon_{\infty} \left( 1 - \frac{\omega_p^2}{\omega^2 + i\omega\gamma_{\text{ENZ}}} \right) \quad (1)$$

where  $\epsilon_{\infty}$  is given by the Sellmeier's equation for InGaAs,  $\omega_p$  is the plasma frequency, and  $\gamma_{\text{ENZ}}$  is the damping rate. The monochromatic time harmonic convention,  $\exp(-i\omega t)$ , is implicitly assumed. Since the plasma frequency is proportional to the doping density, the ENZ crossing point can be tuned by varying the doping density. The ISTs are described by anisotropic Lorentzian oscillators with (relative) dielectric tensor given as  $\epsilon_{\text{IST}} = \epsilon_t(\hat{x}\hat{x} + \hat{y}\hat{y}) + \epsilon_z\hat{z}\hat{z}$ , with  $\epsilon_t = 10.97$  and

$$\epsilon_z = \epsilon_t + \frac{f_z \omega_0^2}{\omega_0^2 - \omega^2 - 2i\omega\gamma_{\text{IST}}} \quad (2)$$

where  $\omega_0 = 2\pi \times 24.2 \times 10^{12}$  rad/s is the IST angular frequency;  $2\gamma_{\text{IST}}$  represents the IST damping rate, with  $\gamma_{\text{IST}} = 2\pi \times 10^{12}$  rad/s; and  $f_z = 1.2$  is proportional to the IST oscillator strength, the doping density and intersubband matrix elements as described in [23].

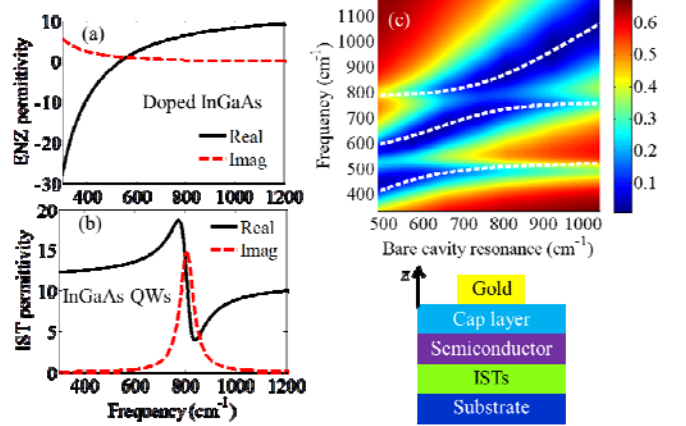


Fig. 3. Numerical results of strong coupling between MMs and detuned ENZ and IST frequencies. (a) Real and imaginary parts of the permittivity of doped InGaAs with the ENZ frequency at  $\sim 600$   $\text{cm}^{-1}$ . (b) Real and imaginary parts of the permittivity of InGaAs quantum wells with the IST dipole transition at  $\sim 800$   $\text{cm}^{-1}$ . (c) Transmittance map from full-wave simulations of gold dogbone resonators on top of a semiconductor heterostructure with detuned ENZ mode and IST transition frequencies. Note the formation of three polariton branches as in the case of optical phonons in Fig. 2. The dotted lines representing the three polariton branches are shown as guides to the eye. The inset shows the side view of the sample.

We analyze in this section the case where the ENZ mode frequency ( $\sim 600$   $\text{cm}^{-1}$ ) is detuned from the IST transition frequency ( $\sim 800$   $\text{cm}^{-1}$ ). The permittivities of the two layers are shown in Fig. 3(a) and Fig. 3(b), which clearly show the ENZ crossing and the IST resonance, respectively. Figure 3(c) shows the transmittance maps obtained from full-wave simulations of an array of dogbone resonators on top of a doped semiconductor layer and a multi-quantum well layer as a function of the bare cavity resonance. We observe clearly that the transmittance spectra exhibit three polariton branches, a signature of strong coupling of the MM resonators to an ENZ mode (around 600  $\text{cm}^{-1}$ ) that is detuned from the ISTs (around 800  $\text{cm}^{-1}$ ). This is very similar to what observed in Fig. 2 for MMs strongly coupled to optical phonons supported by semiconductor nanolayers.

As mentioned earlier, the implementation presented in Fig. 3 is fully engineerable, i.e. the resonance frequencies of the ENZ and dipole layers can be adjusted independently. We further analyze this property in the next section.

### 4. Case 3: Fully engineerable system with overlapping ENZ mode and IST frequencies

A more interesting effect is achieved using the MM/ENZ/IST structure in the inset of Fig. 3 when the doping of the ENZ layer is increased so that the frequency of the ENZ mode coincides with the ISTs resonant frequency ( $\sim 800 \text{ cm}^{-1}$ ) (see Fig. 4(a), which clearly shows the ENZ crossing at  $\sim 800 \text{ cm}^{-1}$ ). We analyze this system for three thicknesses of the ENZ layer (the quantum well thickness is kept constant). The resulting transmittance maps for the three cases are shown in Fig. 4(b-d) which reveal that *only two polariton branches* are

present in this configuration. This is in stark contrast to the three polariton branches observed in Fig. 3(c) for detuned ENZ mode and IST resonance frequencies. We find that the MM/ENZ/IST system exhibits a larger Rabi splitting than when the MM resonators are only coupled to the ENZ mode or the ISTs. Furthermore, Fig. 4(e) shows that the Rabi splitting increases as the thickness of the ENZ layer is increased.

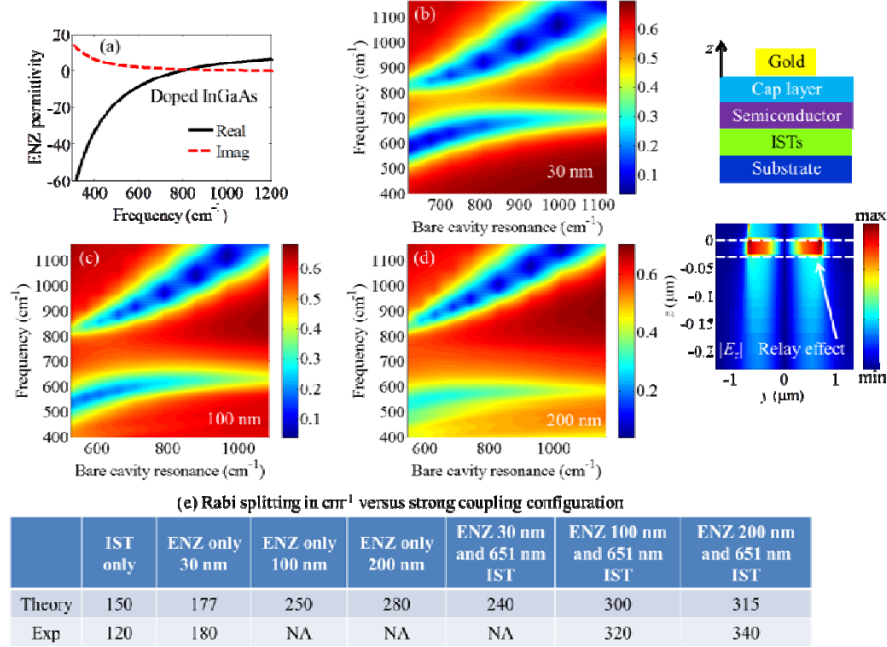


Fig. 4. Numerical results of strong coupling in the MM/ENZ/IST system for the case of degenerate ENZ and IST frequencies. (a) Real and imaginary parts of the permittivity of doped InGaAs with the ENZ crossing at  $\sim 800 \text{ cm}^{-1}$ . (b-d) Full wave simulation transmittance maps for an array of dogbone resonators on top of a semiconductor heterostructure with overlapping ENZ mode and IST resonance frequencies for ENZ layer thicknesses of: (b) 30 nm; (c) 100 nm; and (d) 200 nm. The inset shows the side view of the sample and  $|E_z|$  field relay effect. (e) Experimental and theoretical values for the Rabi splitting (as the spectral difference between the two transmittance dips when the resonances are all overlapping) versus strong coupling configuration: IST only, ENZ only, and both IST and ENZ. The last always shows the largest splitting.

The increase of the Rabi splitting with increasing ENZ layer thickness for the combined ENZ layer/IST layer can be understood by considering the dispersion of the ENZ modes of this combined stack (shown in Fig. 5(a)). Here we analyze a stack consisting of a doped  $\text{In}_{0.53}\text{Ga}_{0.47}\text{As}$  layer with a plasma frequency at  $\sim 800 \text{ cm}^{-1}$ ; a quantum well slab supporting ISTs at a frequency of  $\sim 800 \text{ cm}^{-1}$ ; and an InP substrate. We compute the dispersion of the modes in the complex-frequency/real-wavenumber plane and show it in Fig. 5(b). One can see that for the three ENZ layer thicknesses considered, the modes of the combined stack exhibit a rather flat dependence on the wavenumber, confirming that they behave as ENZ modes similar to those of a single slab [13-15]. This in turn shows that the semiconductor stack in Fig. 5(a) effectively behaves as a “thicker” ENZ structure, leading to an enhanced Rabi splitting. A similar effect was used in Ref. [25] to obtain ultra-strong coupling thanks to a complete overlap between the photon mode and the matter polarization. A similar Rabi splitting increase with thickness was also observed in Ref. [35].

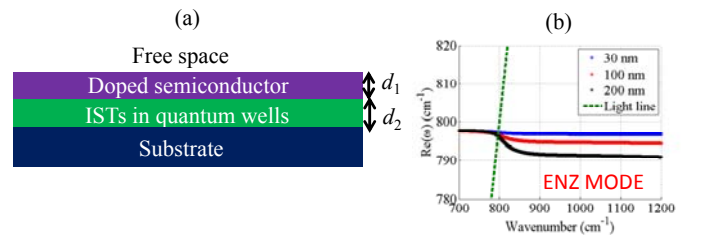


Fig. 5. (a) Semiconductor heterostructure for which we compute the dispersion of the ENZ modes. (b) Real part of the ENZ mode dispersions for the semiconductor heterostructures in (a) with ENZ layer thicknesses of 30, 100 and 200 nm. Note the relatively flat dispersion of  $\text{Re}(\omega)$  versus wavenumber for all the ENZ layer thicknesses.

We also note that the ENZ mode plays a fundamental role in these effects: while, in general, the enhanced field generated below the paddles of the dogbones decays exponentially with distance away from the metamaterial resonators, a thin layer supporting ENZ modes acts as a *relayer* of  $E_z$  fields [13-15]. Due to boundary conditions of the ENZ layer, the field is enhanced and kept constant within the ENZ layer [13-15], so that it is relayed from the top interface to the bottom interface. This field relay effect can

clearly be seen in the inset of Fig. 4, which shows the  $|E_z|$  in the  $y$ - $z$  plane at  $1000\text{ cm}^{-1}$  for the sample of Fig. 4(b) with scaling factor 1.0. The top and bottom ENZ interfaces are depicted by white dashed lines in this figure. On these grounds, we note that the use of an ENZ layer is beneficial as it helps alleviate the field penetration depth limitations mentioned in Ref. [20], provided the overall thickness is within the existence condition of ENZ modes [13-15]. Therefore, the best strategy to maximize the Rabi splitting in a metasurface/semiconductor system is to use a combination of a doped layer supporting an ENZ feature and a layer supporting ISTs, with overlapping ENZ and IST frequencies.

To confirm the predictions of Fig. 4(c-d), we fabricated MM samples for ENZ layer thicknesses of 100 and 200 nm. Figure 6 shows an SEM image of a MM for the 200 nm case and for a MM scaling factor 1.3, along with an image of a single dogbone resonator. The experimental transmittance maps of the two samples are shown in Fig. 6. As predicted in Fig. 4(c-d), we obtain only two polariton branches and a large Rabi splitting. The minor disagreement between the simulations and measurements can be attributed to fabrication imperfections.

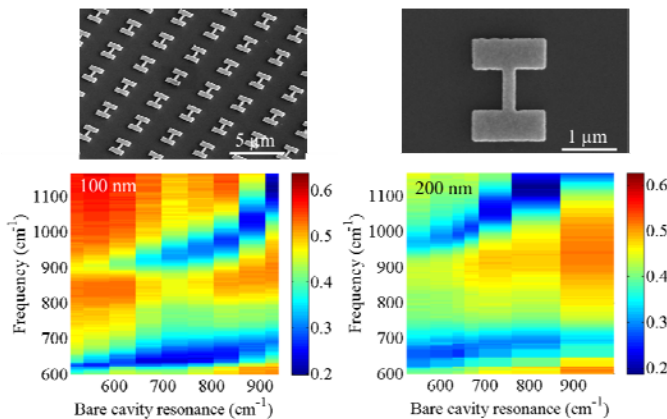


Fig. 6. Experimental transmittance maps for strong coupling in the MM/ENZ/IST system for degenerate ENZ and IST frequencies, with ENZ layer thicknesses of 100 and 200 nm. Note the good agreement between experimental data and simulation results in Fig. 4(c-d). The insets show SEM images of an MM sample and a single resonator fabricated with electron-beam lithography.

## 5. Conclusion

In conclusion, we have demonstrated a platform for tailoring light-matter interactions that employs fundamental excitations in condensed matter such as plasmons and phonons. In particular we design the system's spectral response by creating ENZ modes in semiconductor nanolayers and controlling their interaction with multiple, distinct dipole resonant systems. We have shown examples of this behavior for three-way strongly coupled systems of ENZ modes, phonons, and metamaterials, as well as three-way systems of ENZ modes, quantum well ISTs, and metamaterials. The three-way coupling in these systems results in double and triple polariton branches in transmission spectra. In regards to

the double polariton branches case, we find that the best strategy to maximize the Rabi splitting is to use a combination of a doped layer supporting an ENZ feature and a layer supporting ISTs, with overlapping ENZ and IST frequencies. The flexibility of tuning resonance frequencies and couplings renders this platform attractive for low-voltage tunable filters, light-emitting diodes, and efficient nonlinear composite materials.

## Acknowledgment

The authors acknowledge fruitful discussions with Prof. Francois Marquier, Institut d'Optique, France. This work was supported by the U.S. Department of Energy, Office of Basic Energy Sciences, Division of Materials Sciences and Engineering and performed, in part, at the Center for Integrated Nanotechnologies, an Office of Science User Facility operated for the U.S. Department of Energy (DOE) Office of Science. Sandia National Laboratories is a multi-program laboratory managed and operated by Sandia Corporation, a wholly owned subsidiary of Lockheed Martin Corporation, for the U.S. Department of Energy's National Nuclear Security Administration under contract DE-AC04-94AL85000.

## References

1. N. Engheta, "Pursuing Near-Zero Response," *Science* **340**, 286-287 (2013).
2. M. Silveirinha, and N. Engheta, "Tunneling of Electromagnetic Energy through Subwavelength Channels and Bends using  $\epsilon$ -Near-Zero Materials," *Physical Review Letters* **97**, 157403 (2006).
3. R. Liu, Q. Cheng, T. Hand, J. Mock, T. Cui, S. Cummer, and D. Smith, "Experimental Demonstration of Electromagnetic Tunneling Through an Epsilon-Near-Zero Metamaterial at Microwave Frequencies," *Physical Review Letters* **100**, 023903 (2008).
4. D. Adams, S. Inampudi, T. Ribaudo, D. Slocum, S. Vangala, N. Kuhta, W. Goodhue, V. Podolskiy, and D. Wasserman, "Funneling Light through a Subwavelength Aperture with Epsilon-Near-Zero Materials," *Physical Review Letters* **107**, 133901 (2011).
5. K. C. Gupta, "Narrow-beam antennas using an artificial dielectric medium with permittivity less than unity," *Electronics Letters* **7**, 16-18 (1971).
6. S. Enoch, G. Tayeb, P. Sabouroux, N. Guérin, and P. Vincent, "A Metamaterial for Directive Emission," *Physical Review Letters* **89**, 213902 (2002).
7. G. Lovat, P. Burghignoli, F. Capolino, D. R. Jackson, and D. R. Wilton, "Analysis of directive radiation from a line source in a metamaterial slab with low permittivity," *Antennas and Propagation, IEEE Transactions on* **54**, 1017-1030 (2006).
8. A. Alù, M. G. Silveirinha, A. Salandrino, and N. Engheta, "Epsilon-near-zero metamaterials and electromagnetic sources: Tailoring the radiation phase pattern," *Physical Review B* **75**, 155410 (2007).
9. N. Engheta, "Circuits with Light at Nanoscales: Optical Nanocircuits Inspired by Metamaterials," *Science* **317**, 1698-1702 (2007).
10. C. Argyropoulos, P.-Y. Chen, G. D'Aguanno, N. Engheta, and A. Alù, "Boosting optical nonlinearities in  $\epsilon$ -near-zero plasmonic channels," *Physical Review B* **85**, 045129 (2012).
11. D. de Ceglia, S. Campione, M. A. Vincenti, F. Capolino, and M. Scalora, "Low-damping epsilon-near-zero slabs: Nonlinear and nonlocal optical properties," *Physical Review B* **87**, 155140 (2013).
12. A. Monti, F. Bilotti, A. Toscano, and L. Vegni, "Possible implementation of epsilon-near-zero metamaterials working at optical frequencies," *Optics Communications* **285**, 3412-3418 (2012).
13. S. Vassant, J. P. Hugonin, F. Marquier, and J. J. Greffet, "Berreman mode and epsilon near zero mode," *Opt Express* **20**, 23971-23977 (2012).
14. S. Vassant, A. Archambault, F. Marquier, F. Pardo, U. Gennser, A. Cavanna, J. L. Pelouard, and J. J. Greffet, "Epsilon-Near-Zero Mode for Active Optoelectronic Devices," *Physical Review Letters* **109**, 237401 (2012).

15. S. Campione, I. Brener, and F. Marquier, "Theory of epsilon-near-zero modes in ultrathin films," *Physical Review B* **91**, 121408 (2015).
16. P. Jouy, A. Vasanelli, Y. Todorov, A. Delteil, G. Biasiol, L. Sorba, and C. Sirtori, "Transition from strong to ultrastrong coupling regime in mid-infrared metal-dielectric-metal cavities," *Appl. Phys. Lett.* **98**, 231114-231113 (2011).
17. A. Delteil, A. Vasanelli, Y. Todorov, C. Feuillet Palma, M. Renaudat St-Jean, G. Beaudoin, I. Sagnes, and C. Sirtori, "Charge-Induced Coherence between Intersubband Plasmons in a Quantum Structure," *Physical Review Letters* **109**, 246808 (2012).
18. G. Scalari, C. Maissen, D. Hagenmuller, S. De Liberato, C. Ciuti, C. Reichl, W. Wegscheider, D. Schuh, M. Beck, and J. Faist, "Ultrastrong light-matter coupling at terahertz frequencies with split ring resonators and inter-Landau level transitions," *J. Appl. Phys.* **113**, 136510-136515 (2013).
19. D. Dietze, A. Benz, G. Strasser, K. Unterrainer, and J. Darmo, "Terahertz meta-atoms coupled to a quantum well intersubband transition," *Opt. Express* **19**, 13700 (2011).
20. A. Benz, S. Campione, S. Liu, I. Montano, J. F. Klem, A. Allerman, J. R. Wendt, M. B. Sinclair, F. Capolino, and I. Brener, "Strong coupling in the sub-wavelength limit using metamaterial nanocavities," *Nat Commun* **4**, 2882 (2013).
21. S. Campione, A. Benz, J. F. Klem, M. B. Sinclair, I. Brener, and F. Capolino, "Electrodynamic modeling of strong coupling between a metasurface and intersubband transitions in quantum wells," *Physical Review B* **89**, 165133 (2014).
22. A. Gabbay, and I. Brener, "Theory and modeling of electrically tunable metamaterial devices using inter-subband transitions in semiconductor quantum wells," *Opt. Express* **20**, 6584 (2012).
23. A. Gabbay, J. Reno, J. R. Wendt, A. Gin, M. C. Wanke, M. B. Sinclair, E. Shaner, and I. Brener, "Interaction between metamaterial resonators and intersubband transitions in semiconductor quantum wells," *Appl. Phys. Lett.* **98**, 203103-203103 (2011).
24. Y. C. Jun, J. Reno, T. Ribaudou, E. Shaner, J.-J. Greffet, S. Vassant, F. Marquier, M. Sinclair, and I. Brener, "Epsilon-Near-Zero Strong Coupling in Metamaterial-Semiconductor Hybrid Structures," *Nano Letters* **13**, 5391-5396 (2013).
25. B. Askenazi, A. Vasanelli, A. Delteil, Y. Todorov, L. C. Andreani, G. Beaudoin, I. Sagnes, and C. Sirtori, "Ultra-strong light-matter coupling for designer Reststrahlen band," *New Journal of Physics* **16**, 043029 (2014).
26. D. J. Shelton, I. Brener, J. C. Ginn, M. B. Sinclair, D. W. Peters, K. R. Coffey, and G. D. Boreman, "Strong Coupling between Nanoscale Metamaterials and Phonons," *Nano Letters* **11**, 2104-2108 (2011).
27. F. Neubrech, D. Weber, D. Enders, T. Nagao, and A. Pucci, "Antenna Sensing of Surface Phonon Polaritons†," *The Journal of Physical Chemistry C* **114**, 7299-7301 (2010).
28. A. Benz, I. Montano, J. F. Klem, and I. Brener, "Tunable metamaterials based on voltage controlled strong coupling," *Applied Physics Letters* **103**, 263116 (2013).
29. S. Campione, A. Benz, M. B. Sinclair, F. Capolino, and I. Brener, "Second harmonic generation from metamaterials strongly coupled to intersubband transitions in quantum wells," *Applied Physics Letters* **104**, - (2014).
30. J. Lee, M. Tymchenko, C. Argyropoulos, P.-Y. Chen, F. Lu, F. Demmerle, G. Boehm, M.-C. Amann, A. Alu, and M. A. Belkin, "Giant nonlinear response from plasmonic metasurfaces coupled to intersubband transitions," *Nature* **511**, 65-69 (2014).
31. O. Wolf, S. Campione, A. Benz, A. P. Ravikumar, S. Liu, T. S. Luk, E. A. Kadlec, E. A. Shaner, J. F. Klem, M. B. Sinclair, and I. Brener, "Phased-Array Sources Based on Nonlinear Metamaterial Nanocavities," *Nature Communications* **6**, 7667 (2015).
32. M. Geiser, G. Scalari, F. Castellano, M. Beck, and J. Faist, "Room temperature terahertz polariton emitter," *Appl. Phys. Lett.* **101**, 141118 (2012).
33. M. A. Ordal, L. L. Long, R. J. Bell, S. E. Bell, R. R. Bell, J. R. W. Alexander, and C. A. Ward, "Optical properties of the metals Al, Co, Cu, Au, Fe, Pb, Ni, Pd, Pt, Ag, Ti, and W in the infrared and far infrared," *Appl. Opt.* **22**, 1099-1119 (1983).
34. FDTD Solutions by FDTD Lumerical Inc. <https://www.lumerical.com/>.
35. A. Benz, S. Campione, S. Liu, I. Montano, J. F. Klem, M. B. Sinclair, F. Capolino, and I. Brener, "Monolithic metallic nanocavities for strong light-matter interaction to quantum-well intersubband excitations," *Opt. Express* **21**, 32572-32581 (2013).